Institute of Physics and Astronomy
University of Aarhus
Ny Munkegade
8000 Århus C
Denmark

November 20, 1997

Progress Report

On the Nature of high HI Column Density Quasar Absorption Line Systems at high Redshifts

Johan P. U. Fynbo

Contents

Preface

In this progress report I discuss the results of work done during my first two years of study for the degree of PhD. My PhD is an observational study of the high column density Quasar Absorption Line Systems at high redshifts. The work presented here has been done in collaboration with my external supervisor Dr. Palle Møller, currently at STScI, and Dr. Stephen J. Warren, Imperial College, London. Unless otherwise stated, the work presented here has been performed by me under the supervision of Palle Møller and my local supervisor Dr. Bjarne Thomsen. In chapter 4 I describe the projects which will be performed during part B of my PhD study in collaboration between Palle Møller, Bjarne Thomsen, and myself.

I start this progress report with an introduction to the study of Quasar Absorption Line Systems. I then continue with a description of the projects I have been working on during my first two years. Finally I present an outlook to the projects that will be performed during the remaining two years of my PhD study.

Chapter 1

Introduction

1.1 The Lyα forest

The basic frame work of this study is structure formation in the universe. One of the most important scientific discoveries of this century is that of the cosmic microwave background radiation with the results from the COBE mission showing that the universe, at the time when radiation decoupled from matter, was very homogeneous (see for example [1].) The aim of the study of structure formation is to gain insight into how the the universe evolved from this very homogeneous state to the clumpy universe we see today containing large walls, clusters, galaxies, planets and people.

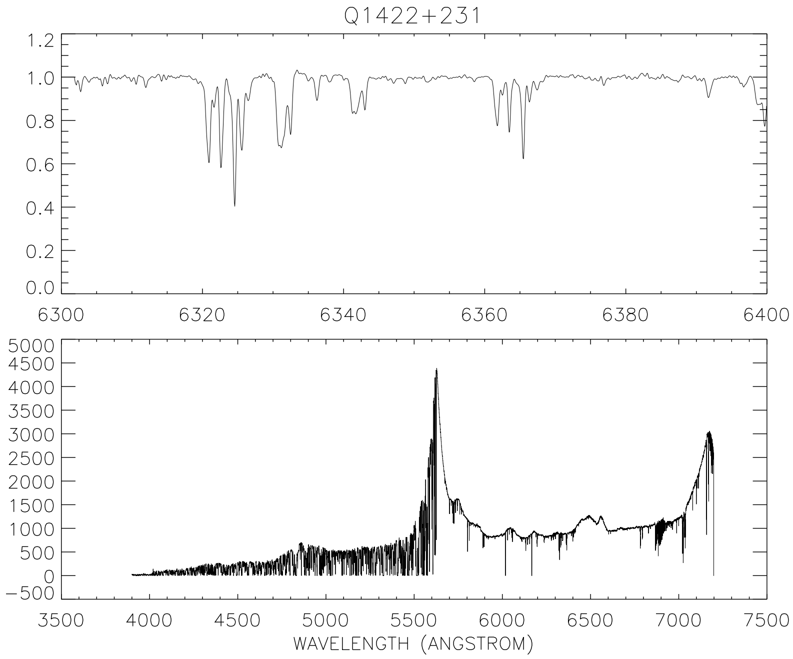

Figure 1.1: The spectrum of Q1422+231 from [2]. The units on the y-axis are flux units.

One very promising method to obtain observational insight into this evolution is based on the study of absorption lines in the spectra of high redshift Quasi-Stellar Objects (QSOs). These absorption lines are due to gas clouds, refered to as Quasar Absorption Line Systems (QALS), intersecting the line of sight to the underlying QSOs. For example Fig. 1.1 shows a high signal-to-noise spectrum of the z=3.6 QSO Q1422+231 [2]. The emission line at 5590Å, seen in the lower panel, is Lyα from the QSO. Bluewards of this can be seen a very large number of absorption lines, with almost all the lines in this region due to neutral hydrogen in clouds along the line of sight to the QSO. These QALS are denominated 'the Lyα forest'. The lines in the region redwards of the Lyα emission line, of which a 100Å region is shown in the upper panel, are due to metal ions, mainly CIV and SiIV, associated with some of the stronger Lyα systems. The origin of these systems is believed to be extended galactic halos.

Fig. 1.2 shows the number of clouds per unit z and unit HI column density (N_{HI}) as a function of N_{HI} from a study by Hu et al. [3]. As seen, QALS are detected with N_{HI}

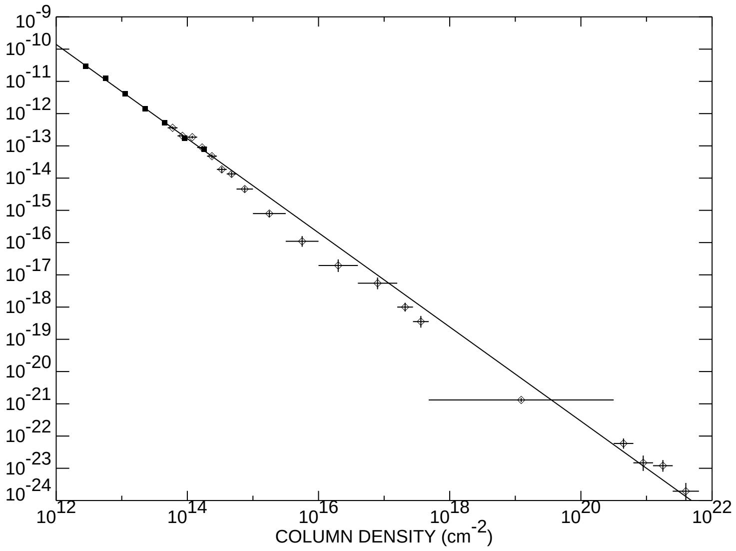

Figure 1.2: The number of clouds per unit z and unit N_{HI} as a function of N_{HI}. The units on the y-axis are cm^{-2}.

ranging from $10^{12.5}$ cm^{-2} to $10^{21.8}$ cm^{-2}. At a redshift of 3, $N_{HI} = 10^{12.5}$ cm^{-2} corresponds to a baryonic overdensity smaller than 1 for a structure of dimensions $\approx$ 100 kpc, whereas, $N_{HI} = 10^{21}$ cm^{-2} corresponds to the column density of mass in stars and gas in the Galaxy. QALS are found from redshifts z $\approx$ 0 to z $>$ 4.5 [5], [6], [7]. In nearly all systems with HI column densities larger than 10^{15} cm^{-2} one finds associated metal absorption due mainly to SiIV and CIV [8]. As N_{HI} rises above 10^{19} cm^{-2}, many low ionization lines due to metals appear. Hence QALS provide a wealth of information for a study of structure formation and evolution of element composition for a wide range of systems; from very dilute clouds only slightly denser than the mean, to very dense clouds with column densities similar to those of present day galaxies, and also from when the universe was less than 10% of its age to the present day.

1.2 High Column density QALS

The subject of my PhD project is the nature of the rare high HI column density QALS seen in the lower right corner of Fig. 1.2. Primarily the study is concerned with the so called Damped Lyα Absorbers (DLA), which by definition have $N_{HI} > 2\text{x}10^{20}$ cm^{-2}. An example of an absorption line caused by a DLA at the redshift z = 2.8268 towards the z = 3.2 QSO Q1425+6039 is shown in Fig. 1.3 [9]. A broad absorption trough centred at 4652 Å, which is

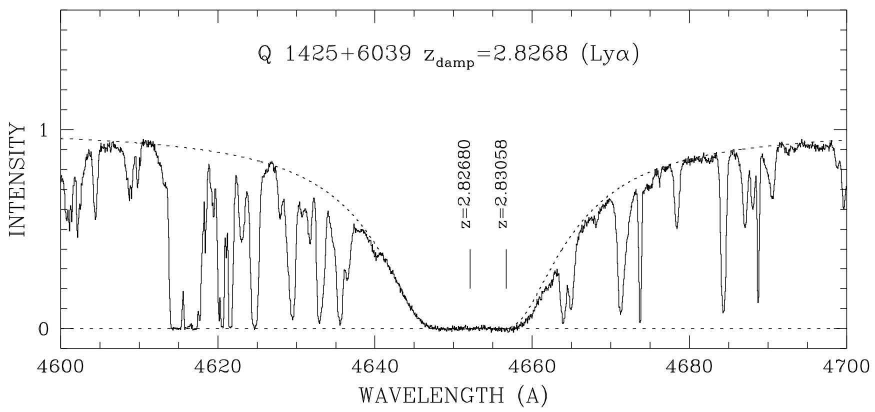

Figure 1.3: The damped Lyα line in the spectrum of Q1425+6039. The dotted line shows a fit to the data for $N_{HI} = 2\text{x}10^{20}$ cm^{-2}.

the wavelength of redshifted Lyα (1215.67Å), can be seen. DLAs owe their name to the broad damping wings seen on the sides of the trough. The column density of this absorber is N_{HI} = $2\text{x}10^{20}$ cm^{-2}. The other redshift indicated (z = 2.83058) is that of a second component having $N_{HI} = 1\text{x}10^{19}$ cm^{-2}. In this case one finds the following associated metal absorption lines : CII, CIV, NI, AlII, SiII, SiIV, FeII and NII.

1.3 Testing Cosmological models with DLAs

Recently DLAs have been used directly to test different cosmological models for structure formation. A key ingredient in a modern structure formation recipe is dark matter, and given the primordial fluctuation spectrum the main difference between models is the nature of the dark matter. The occurrence of DLAs as a function of time in the models is strongly dependent on the nature of the dark matter. Using this, Gardner and collaborators [4] have tested a large number of models and find that only the Cold Dark Matter model (CDM) fits the data. These results are still preliminary, but without any doubt in the near future this will prove to be a very strong test of models of structure formation.

1.4 The nature of DLAs

At the present time approximately 100 DLA systems are listed in the literature [5], [6], [7]. From studies of the spectra of the underlying QSOs, much information about the metallicity and gas dynamics of the DLAs has been obtained, see e.g. [9], but very little about their sizes and morphologies is known. The question is : what was the nature of galaxies in the young universe? It is a long standing controversy whether DLAs are large spiral discs in formation or rather small galaxy subunits that later, through merging, build up the galaxies we see today, see for example [10] and references therein.

To find a solution we need to gain more information which can be drawn from absorption lines in the spectra of the underlying QSOs. Various methods have been used to obtain observational evidence for the nature of DLAs; the obvious method being imaging.

1.5 Narrow band imaging

The technique which we use is narrow band imaging. By performing narrow band imaging in a filter tuned to Lyα at the redshift of the absorber one circumvents the problem of the strong emission from the QSO. Remember that we try to see a faint galaxy 0–3 arcsec from a typically much brighter QSO. However, due to the damped absorption line the QSO emission will be almost completely absent in the narrow band image making the DLA itself, if it is a Lyα *emitter*, stand out. If DLAs experience ongoing star formation and if they contain little or no dust, we expect to see Lyα emission.

Much telescope time has been dedicated to the narrow band imaging of DLAs over the past decade, e.g. [11] and references therein, but so far resulting in only a single confirmed detection [12], [13]. In addition, a spectroscopically confirmed broad band detection [14] and a purely spectroscopic detection of Lyα emission have been reported [15], as well as a number of DLA candidates, which have not been confirmed by spectroscopy [16], [17], [18].

The main goal of my PhD project is to look for Lyα emission from more DLAs.

1.6 Lyman-break Galaxies

I end this introduction by describing a completely different approach to the observational study of high redshift galaxies, which has recently proved quite successful. This method is based on broad band imaging in a filter set that is designed to identify star forming galaxies at redshifts above 3. In the spectrum of star forming galaxies there will be a strong discontinuity at the Lyman limit resulting in virtually no emission bluewards of the rest wavelength 912 Å. This technique has now led to the discovery of hundreds of galaxies in the range z = 2–4, see [27] and references therein. The fact that these galaxies are detected independently with completely different selection criteria than the DLAs makes it very interesting to compare those two samples of high redshift galaxies and thus hopefully reach a more complete understanding of young galaxies and galaxy formation.

Chapter 2

Galaxies in the field of PKS0528–250

2.1 The field of PKS0528–250

In 1993, Palle Møller and Stephen Warren published the first detection of Lyα emission from a DLA confirmed by both imaging and spectroscopy [12], [13]. This was from the z = 2.81 DLA towards PKS0528–25, subsequently called S1. Besides from S1 the authors found Lyα emission from two other galaxies, called S2 and S3, at the same redshift as the DLA. In 1995 they obtained 30 orbits of HST-WFPC2 data (Hubble Space Telescope - Wide Field Planetary Camera 2) on the field.

The main purpose of the first project in my PhD-study was to make full use of these 30 orbits of HST data. The spectrum of PKS0528–250 is very rich in high column density QALS, in that, besides the damped Lyα absorption line at z=2.81 it has another damped Lyα absorption line at z=2.14, a Lyman limit absorber at z=2.54, and a MgII absorber at z=0.94 [32], [33]. Our goal was, from the HST-imaging and photometry to find some candidate galaxies associated with the absorption systems at z=0.94, z=2.14, z=2.54 and z=2.81 and then to do follow-up spectroscopy on these candidates.

Palle Møller, Stephen J. Warren, Paul Francis and I were, in the autumn of 1996, granted 2 nights on the Anglo Australian Telescope (AAT) (Principal Investigator (PI) Francis) and 3 nights on the ESO 3.6 m telescope (PI Møller) for Multi Object Spectroscopy (MOS) for this study.

In the following I describe the observations, reduction of the data, selection of candidate medium and high redshift galaxies and the preparation of masks for the MOS.

2.2 HST-Observations and Reduction

For a thorough description of the HST-observations see [34]. The observations were done in three filters : the WFPC2 standard I (F814W) and B (F450W) and the medium-passband (width 177Å) filter F467M, subsequently called M. The reason for choosing F467M is that

Date	Filter	Band	Exposure (sec)
1995 Feb 2	F467M	M	12900
1995 Mar5	F467M	M	12900
1995 Mar8	F814W	I	12900
1995 Mar8	F450W	B	12900
1995 Mar9	F467M	M	12900

Table 2.1: Journal of HST observations

the Lyα emission line will be inside this filter for $2.78 < z < 2.9$.

The journal of observations appears in Table 2.1. Each of the five visits listed in Table 2.1 were built up by 6 exposures so that we have 6 exposures in I, 6 in B and 18 exposures in M.

The frames were combined using a code developed by Palle Møller. This code adds the individual frames using sigma-clipping to remove cosmic ray hits and weighting each frame by its sky-variance. It combines the frames using half-integer pixel shifts thereby improving the resolution of the final combined frame. This is done in order to compensate for the fact that the Wide Field CCDs undersample the Point Spread Function (PSF) of HST.

2.3 Photometry

2.3.1 Zero-points for HST-photometry

We chose to work in the UBVRI system since we want to compare with ground based data. The zero-points needed to obtain I-magnitudes from F814W count rates and B-magnitudes from F450W count rates are given in [35] (their Table 9). The correspondence between I and F814W is better than 0.05 mag for 0<V-I<3. For F450W the difference from B is -0.2 at B-V=-0.8 and 0.4 at B-V=2. The authors also provide the zero-point for F467M to B. Here the differences changes from -0.5 to 0.5 over the same range in B-V.

2.3.2 Isophote photometry

We have used as well the FOCAS photometry package as SExtractor. We started in the spring of 1996 with FOCAS and completed the photometry of all galaxies in all WF-frames. However, FOCAS detects a large number of objects which are not real. Furthermore, FOCAS is very uncomfortable to work with since it only accepts integer data. Hence the photometry was redone with SExtractor as soon as we became aware of it. For a discussion of SExtractor see [36].

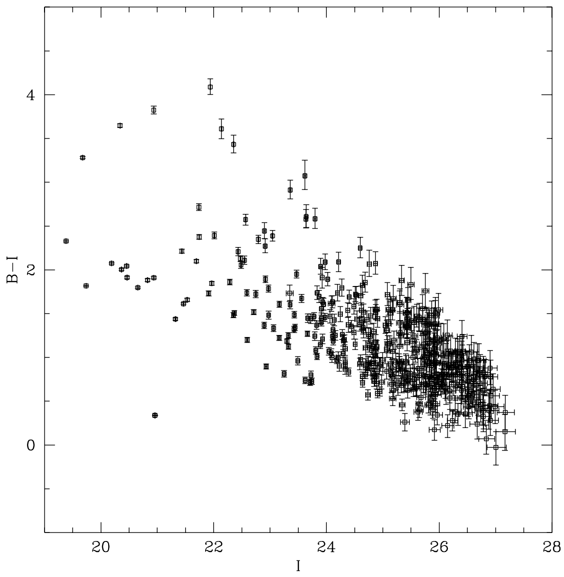

Figure 2.1: Colour magnitude diagram for 430 galaxies in the field of PKS0528–250

What we want to obtain from the photometry-software is 1) a well defined and robust detection of objects in the field, and 2) a measurement of the flux from the detected objects. SExtractor fulfills these demands very well. We will not describe SExtractor in detail, but just give a brief overview of its procedures. SExtractor first determines a background map. Objects are then all collections of a minimum *Minarea* of pixels which are above a given *threshold* of the sky σ. *Minarea* and *threshold* are specified by the user. An option in the detection process is to specify a detection image along with the primary image. SExtractor then extracts the objects from the detection image and performs the photometry on these objects in the primary image. Here we use the sum of the combined images as detection images. Once objects are detected there are various magnitudes one can choose. We use the isophote magnitudes, since we are interested in precise colours of faint galaxies.

2.3.3 Results

SExtractor detected a total of 969 objects in the three WF3 fields. After visual inspection of these objects 112 were discarded as being either stars, diffraction spikes or unreal detections near bright objects. Thus we have detected a total of 857 galaxies.

Fig. 2.1 shows the B-I versus I colour-magnitude diagram for the 430 of these objects which have a mean error in B-I smaller than 0.2 mag. The trend that the galaxies become bluer and bluer with increasing I magnitude is partly real, partly due to the error-criteria, i.e. a selection effect.

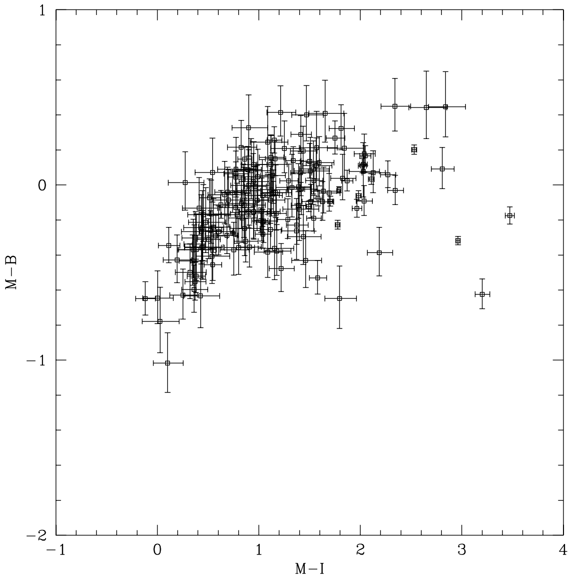

(a) Colour-colour diagram for 140 galaxies in the field of PKS0528–250

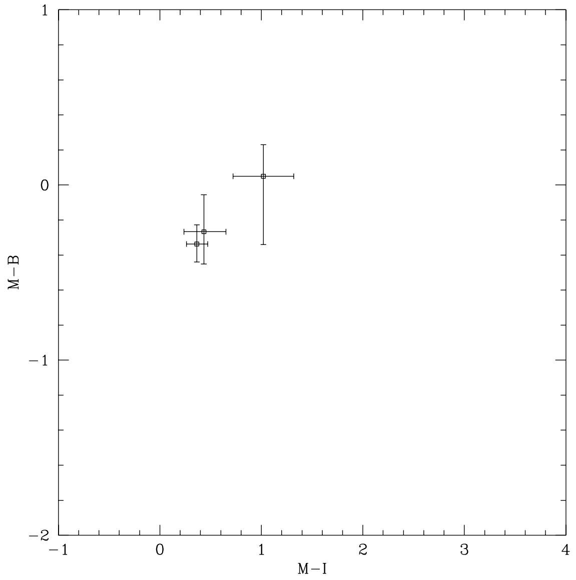

(b) Colour-colour diagram for S1, S2 and S3

Figure 2.2: Colour-colour diagram for galaxies in the field of PKS0528–250

2.4 Selection of candidate high-redshift galaxies

Our job is now to select among the 857 detected galaxies candidate medium and high redshift galaxies. The main interest is galaxies with Lyα emission in the M-filter, i.e. Lyα emitting galaxies at redshifts between z = 2.78 and z=2.9. To identify such galaxies we construct a M–B vs. M–I colour-colour diagram. Blue objects with excess emission in the M filter relative to B should then have a very negative M–B colour and a low M–I colour. Fig. 2.2a shows the M–B versus M–I colour-colour diagram for 140 galaxies with a mean error in M-B smaller than 0.2. Fig. 2.2b shows the positions of S1, S2 and S3 in the diagram. Obviously S1, S2 and S3 do not occupy a special region of the colour-colour diagram, which means that we unfortunately had very little information to use in the selection of candidate high redshift galaxies for further spectroscopic studies. It was later realized why S1, S2 and S3 did not have more negative M–B colours, despite the fact that they have Lyα emission lines in the M-filter. The reason was that the emission contours in M were more extended than in I and B. Thus as we used the sum of the combined images, where the broad band images dominate, as detection image we missed Lyα flux and hence underestimated M–B, see [34].

To try to obtain more understanding of how galaxies distribute in the colour-colour diagram, and hence obtain a better basis for the selection of candidate galaxies, we did the following. From Stephane Charlot we obtained the latest version of the Bruzual and Charlot models for the spectral energy distributions of galaxies [37]. These models do not include

Lyα line emission, so since we wished to see the effect of Lyα line emission we included this by hand in the model-spectra. We assigned (in a rather ad hoc and unphysical way) a Lyα emission to a given galaxy by adding a Gaussian with a width corresponding to 1000km/s and a height equal to 10 times the maximum continuum flux. This very large Lyα line flux will clearly show the effect of Lyα emission in the M-filter. From the STScI ftp-archive we then obtained the transmission curves of the F450W, F467M and F814W filters. Finally using the prescriptions in [38] and [39] to include the effect of blanketing due to intervening Lyα clouds we calculated the colours for a large number of galaxy spectra with ages from 1 million to 17 billion years. For galaxies older than 5 billion years we calculated colours for $0 < z < 1.5$ in steps of 0.1. For younger galaxies we calculated colours for $1 < z < 4$ also in steps of 0.1. Furthermore for the younger galaxies we calculated colours for $2.78 < z < 2.90$, i.e. the range for which the Lyα emission line falls within the M-filter, in steps of 0.01. The resulting colour-colour diagram is shown as Fig. 2.3a. The filled circles represent the young

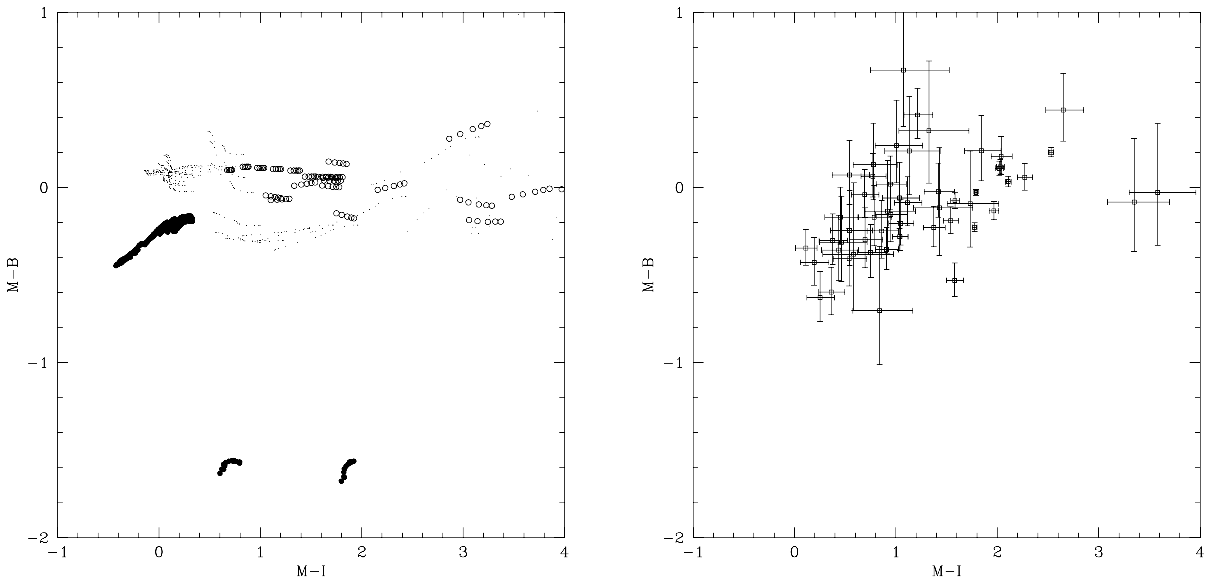

(a) Colour-colour diagram for model galaxies

(b) Colour-colour diagram for candidate high redshift galaxies

Figure 2.3: Colour-colour diagram for model and candidate high redshift galaxies

high redshift galaxies with Lyα emission in M, the open circles represent the low redshift older galaxies, and the dots represent the high redshift galaxies. We see that as expected the galaxies with Lyα emission in the M-filter have negative M–B colour. Some even have M–B as low as $\approx$-1.5. These galaxies are however all older than 1 billion years, so here strong Lyα emission is probably unlikely.

2.5 Multi object Spectroscopy

The next step was in accordance with the results from simulations to choose blue compact galaxies, preferably with a negative M–B colour, compact meaning objects with broad band sizes 0.5 arcsec or smaller. For z=0.94 candidates we mainly chose objects in what appears to be a cluster north west of PKS0528–250.

Most of the autumn of 1996 we used on the preparation of masks for these observing runs, which was certainly not a trivial task. In MOS there will be a slit for each galaxy in the mask. The minimum slit length is 10 arcsec since we need to have some sky within the slit for sky-subtraction. This puts very strict limits on the number of galaxies that can be fitted inside a mask. Fig. 2.3b shows the colours of the candidate galaxies we chose. Besides these galaxies we added a number of bright galaxies from the surrounding fields chosen from ground based data. Finally we chose to put PKS0528–250 itself on two of the masks.

The masks were then produced in the following way. At the AAT we needed for a given mask to provide a list of right ascensions and declinations for the target objects along with the position angle of the mask. After some problems this turned out to be possible, and we obtained two nights of data on two masks in November 1996. At the ESO 3.6m telescope, designing the MOS-masks was somewhat more complicated. These masks are produced in the following way : first one takes a short exposure of the target field with the given position angle in EFOSC imaging mode, then, with a ramtex cursor one clicks at the objects which one wants. However, this was impossible for us, since most of the galaxies would never show up in a short exposure. Hence we did the following. We obtained, about a month in advance from a friendly observer at the 3.6m-telescope, short EFOSC exposures of the field of PKS0528–250 with the three rotations we had decided upon. Then we derived the transformation from the HST-frames to these EFOSC frames and at the position of the target objects we made crosses. These artificial EFOSC-frames we then used for the design of three masks. We obtained three nights of data in December 1996.

The final reduction of these spectroscopic data is expected to be done early in 1998.

Chapter 3

The DLA towards Q0151+048

3.1 Q0151+048 : a $z_{abs} \approx z_{ems}$ absorber

Of the three DLAs with detected Lyα emission in the literature two are at approximately the same redshift as the underlying QSO, namely the DLAs towards PKS0528–250, S1, [12], [13], and Q2059–360 [15]. This fact has led us to try to find and study more such $z_{abs} \approx z_{ems}$ absorbers in the hope that for some reason these systems are more likely to be Lyα emitters. The z = 1.92 QSO Q0151+048 was found to be a very promising candidate. This object is actually a physical QSO pair consisting of relatively bright V = 17.6 component, which we will refer to as qA, at a redshift of 1.922 and an approximately 3 mag fainter neighbour QSO, hereafter qB, at a redshift of 1.937 3.3 arcsec north east of qA. In the spectrum of qA there is a damped Lyα line at z = 1.9342, i.e. it has a *larger* redshift than that of the underlying QSO [19], [20]. This means that the DLA must be moving towards qA with a velocity of at least 1250 km s^{-1}, making the DLA towards qA very similar to the z=2.81 S1 towards the z = 2.79 PKS0528–250 where z_{abs} is also larger than z_{ems}.

In August 1994 S.J. Warren obtained a spectrum of the Lyα region of qA [19]. A careful examination of the damped Lyα absorption line showed excess emission in the bottom of the trough [19]. Hence the field of Q0151+048 was very interesting for a narrow band imaging project; we applied for observing time in the autumn of 1995 (PI Møller) and obtained 5 nights for this project.

3.2 Observations and Data Reduction

Our data was obtained with the Nordic Optical Telescope (NOT) during four nights beginning September 15 1996 (one night was lost due to bad weather.) We chose to image the field in the narrow band filter and in two broad band filters, U and I. The U-filter is needed to obtain narrow–broad band colours that will identify emission line sources in the field, and the purpose of the I band imaging is to help identify eventual low redshift galaxies, which happen to have an emission (e.g. OII) line in the narrow filter. At the beginning of the two first nights we spotted some very diffuse sirius clouds and from our standard star observations we can conclude that these night we not photometric. The last two nights of the observing run were photometric. The seeing ranged from 0.80 arcsec to 1.35 arcsec in the narrow-band frames and from 0.60 arcsec to 1.30 arcsec in the two broad band frames. The CCD used was a 1kx1k back-side illuminated thinned Tektronix with a pixel size 0.176 arcsec and a read noise of $5.4e^{-}$. The Quantum Efficiency (QE) in the UV for this detector rises from 0.3 at λ=0.35μ to 0.6 at λ=0.4μ.

The narrow-band filter was manufactured by Custom Scientific. The filter is tuned to Lyα at a redshift of 1.9342 with a central wavelength λ = 3565Å and a FWHM (Full Width at Half Maximum) of 20Å. The peak transmission of the filter is $T(\lambda)_{max}$ = 0.385, which is probably the best one can obtain in the near UV for a narrow filter. The red leak, i.e. leak of light redder than ≈3600Å is less than 0.0001% out to 1.2 μ. This is important since we want to look for something very faint near the line of sight to the bright qA. The filter transmission curve is shown in Fig. 3.1.

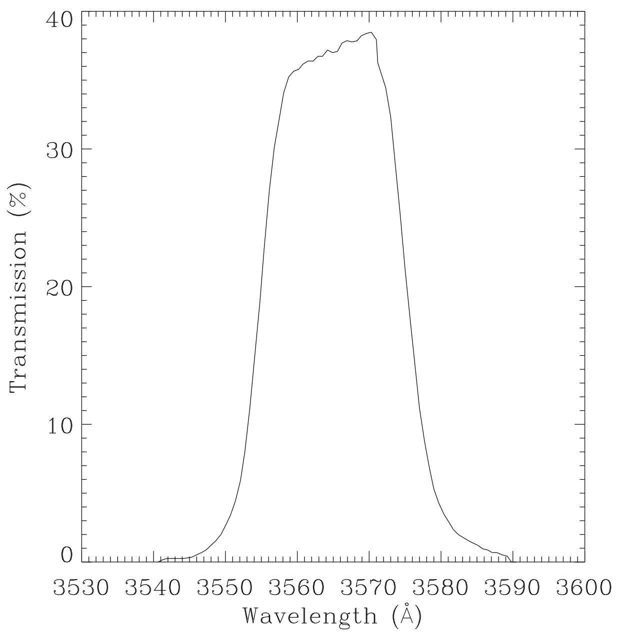

Figure 3.1: The filter transmission curve

Integration times for the narrow-band frames were typically 4000 seconds. This choice is made in a struggle between the Scylla of being dominated by read noise and the Charybdis of having cosmic ray hits all over the CCD frame. Between individual exposures the telescope was moved 2-5 arcsec to minimize the effect of bad pixels. We obtained 17 exposures with a total integration time of 62700 seconds. Bias, dark and twilight flat frames were also obtained. A combined bias image was constructed from 23 bias frames by removing all cosmic ray events, averaging and smoothing. A constant dark current of 1.5 e^{-}/hr was subtracted.

3.2.1 Correction for Scattered Light

At the beginning of the first night of our observing run we realized that light reached the CCD without passing through the filter wheel. This scattered light was not detectable when using broad-band filters, but very significant when using the narrow filter. The scattered light produced a pattern across the upper two third rows of the CCD. The correction for this is described below. We obtained a number of frames with only the scattered light component by using a blocking filter in the filter wheel (a filter with zero transmission.) From these frames we determined a model of the scattered light by median and Gaussian filtering. This model was then scaled and subtracted from the flat frames. These corrected flat frames were then added removing cosmic ray events by median filtering and normalised. The scattered light in the narrow band data frames did not show the same structure across the CCD as in the flat frames, most likely due to a different position of the guide probe used for the guiding of the telescope. Thus we modelled the scattered light in the narrow band data frames by adding all the frames, removing the objects by interpolation and filtering. This model was then scaled to and subtracted from the data frames. After flat fielding all small scale pixel to pixel variations were removed and the large scale variations were less than 5%.

3.2.2 Combination

The corrected frames were then divided in two groups according to seeing: one group of frames with seeing larger than 1 arcsec and one group of frames with seeing less than 1 arcsec. This optimizes the following combination of the frames described below. Both groups were first registered by integer pixel shifts to a common coordinate system and the frames within each group were combined using the optimal combination code described in Møller & Warren, 1993, which maximizes the signal-to-noise ratio for faint sources. Essentially the code adds the frames using sigma-clipping for the removal of cosmic ray events and weights the frames with the sky-variance. The model for the scattered light was included in the calculation of the sky-variance. Finally, the combined frames of the two groups were combined by weighting with the background variance.

Besides the three combined frames we calculated a noise image for each filter containing at a given pixel the variance of that pixel.

Using the broad band U filter we obtained 12000 seconds of integration and 7800 seconds with the I filter. For these data the scattered light was negligible compared to the flux from the sky. In each of the two broad band filters a large number of flat field frames were obtained, and a final flat field was constructed by removal of cosmic ray events, adding and normalising. Finally bias and dark frames were subtracted and the data frames were flat fielded. The frames were then divided into subgroups according to seeing and combined as described above.

3.2.3 Calibration

Also observed in narrow, U and I were three spectrophotometrical standard stars and several Landolt sequences [21]. Standard stars are used for the calibration of the observations.

The calibration of the narrow band data was obtained in the following way. The most reasonable magnitude system for narrow band imaging is the AB system. The AB magnitude at a frequency ν for a given object with flux density F_ν is defined as [22]

$$AB = -48.60 - 2.5\log(F_\nu).$$

We obtained the spectral energy distribution F_λ of the three spectrophotometrical standard stars from the STScI homepage following Colina and Bohlin [23]. We then obtained the AB magnitude for the standards in the narrow filter using

$$AB = -48.60 - 2.5\log(\int_{\lambda_{min}}^{\lambda_{max}} \frac{1}{\lambda_{max} - \lambda_{min}} \frac{F_\lambda(\lambda)\lambda^2}{c} d\lambda),$$

with $\lambda_{min} = 3540$Å and $\lambda_{max} = 3590$Å. Since the spectral energy distributions of the three stars used (BD28d4211, BD25d465 and GD71) are all flat and featureless in the relevant region of the spectrum this simple average is perfectly adequate.

The zero-point and extinction term were then fitted using the measured narrow band instrumental magnitudes of the spectrophotometrical standard stars. For the photometry on the combined narrow band frame of the field of Q0151+048 we first calibrated one of the individual 4000sec exposures obtained at low zenith distance on a photometric night. The magnitudes measured in the combined frame were then transformed to the AB system using the calibrated reference frame. The final standard deviation in the determination of the zero point is estimated to be 0.02 mag.

The calibrations of the U and I filters were obtained in the following way. We first wish to transform our instrumental I and U magnitudes to Johnson U and Cousins I. Hence we fitted zero points and colour terms ((R–I) for I and (U–B) for U) to the measured instrumental magnitudes and the standard magnitudes from [21]. The calibration of the I band data resulted in a small colour term (consistent with zero) as the instrumental I filter was very similar to the standard I filter. In contrast to this the U band calibration resulted in a very large colour term due to the fact that the CCD QE dropped significantly within the U filter. However, including an extra colour term ((U–V)) and only fitting to blue stars produced a reasonable fit. For both U and I filters the estimated error in the zero point is ≈ 0.04 mag. As for the narrow band data we chose reference frames for the photometry on the combined broad band frames. Finally we wish to transform from Johnson U and Cousins I to the AB system. Here we used the transformation given in [24]. From here on we will refer to the narrow, U and I magnitudes thus obtained as u_{AB}, U_{AB} and I_{AB}. U and I will be used for Johnson U and Cousins I respectively.

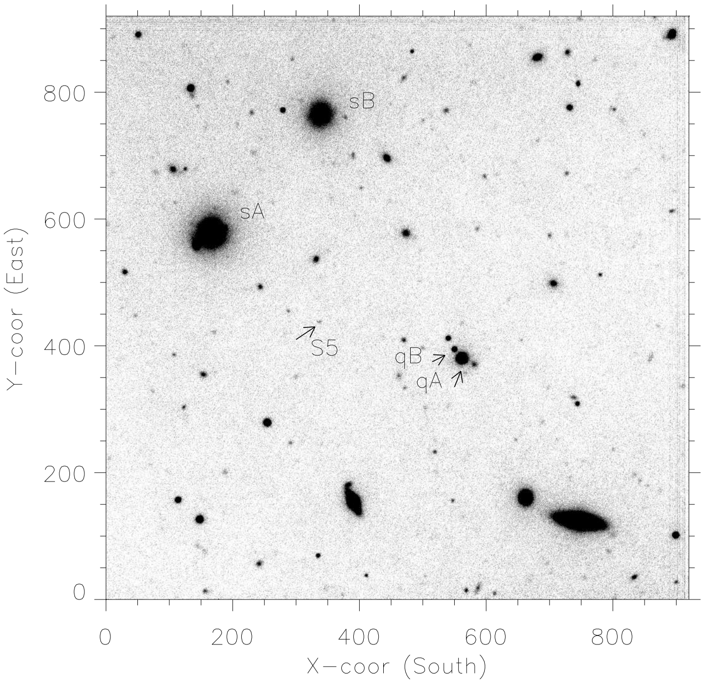

Figure 3.2: Combined I frame containing 920x920 pixels (162x162 arcsec^2) surrounding the quasar pair Q0151+048. North is up and east to the left.

3.3 Results

In Fig. 3.2 we show the final combined I image of 920x920 pixels (162x162 arcsec^2) surrounding Q0151+048. The two QSOs are marked qA and qB. Also marked on the image are two bright stars and a galaxy discussed later. For the two QSOs we find the following magnitudes. For qA I_{AB} = 18.06 and U_{AB} = 17.36, and for qB I_{AB} = 21.07 and U_{AB} = 20.50.

3.3.1 The DLA (S4)

In Fig. 3.3a we show a contour plot of a small section of the combined narrow-band image containing the two quasars. North is up and east to the left. Besides emission from the two quasars, presumedly Lyα from the DLA is seen east of qA. Subtraction of the emission from the two quasars is described below. The two bright stars marked sA and sB in Fig. 3.2 were used with DAOPHOT II (Stetson, 1994) to define a Point Spread Function (PSF). The complex image made up of the extended Ly-alpha emitter super-imposed on the PSFs of the two quasars was decomposed by iteration. First DAOPHOT II was used to fit, and subtract, the two point sources. This was followed by a maximum likelihood fit to the residuals of an exponential disk with free position angle and free axis ratio. The maximum likelihood galaxy model was subsequently subtracted from the original image, and a second iteration of DAOPHOT II fitting to the residuals followed. After 9 rounds of alternating points soruce/exponential disk fitting, the procedure reached a stable solution. This was done by Palle Møller and Stephen Warren.

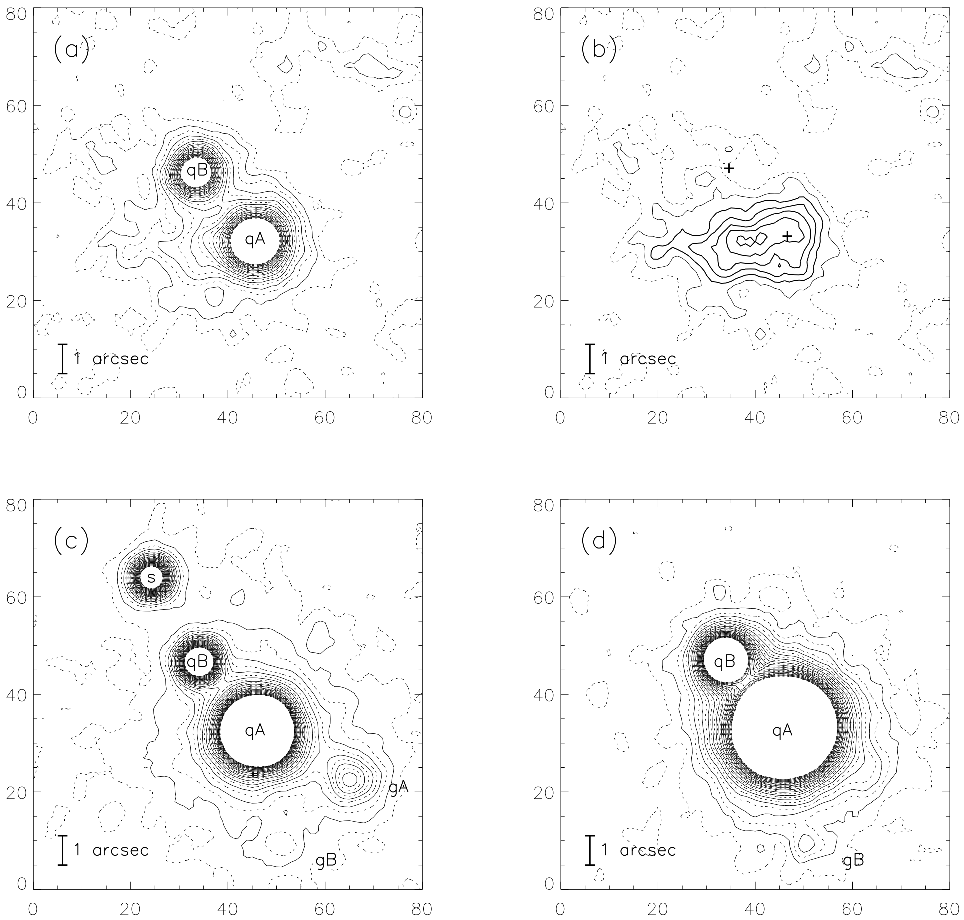

Figure 3.3: 80x80 pixels surrounding Q0151+048. North is up and east to the left. a) and b) is from the narrow-band frame, c) from the I frame and d) from the U-frame.

In Fig. 3.3b the PSFs of the two quasars have been subtracted. Emission is seen from an elongated structure of dimensions 6x3 arcsec^2. In the following we shall refer to this object as S4. We again use SExtractor to perform photometry. With SExtractor we determine the flux of S4 using both the isophotal magnitude aswell as the so called automatic aperture magnitude. The isophotal magnitude simply determines the flux within the detection threshold. The automatic aperture magnitude is intended to give the most precise estimate of the total magnitude. Using the later we find a total flux from S4 of 1.88(4) x 10^{-15} erg cm^{-2} s^{-1} where the error is from the PSF-scaling and PSF-subtraction, photon noise and read-out noise. The dominant noise is the photon noise. From the isophotal magnitude we determine a flux of 1.18(4) x 10^{-15} erg cm^{-2} s^{-1}. The lower panels in Fig. 3.3 shows the same field as the top panels, but for the combined I (c) and U (d) frames respectively. Here we again see the two QSOs qA and qB. In Fig. 3.3c north east of qB there is a red star and south west of qA there are two faint galaxies marked gA and gB. We also tried to do PSF-subtraction in the I band frame, but here we are only able to put a lower limit on the magnitude of S4 (upper limit on the flux). This is because the relative brightness of the QSO and S4 is much larger in the broad band frames where we do not have the damped Lyα absorption line removing most of the QSO emission. The limits we infer for I_{AB} is $I_{AB} > 24$ for a point source 1 arcsec from qA. For an extended source the limit can be significantly lower. In the U band frame we do see some residual flux. The U_{AB} magnitude for this emission is $U_{AB} \approx 22$. However, we have not yet established the significance of this. This point will be addressed further in chapter 4.

3.3.2 Narrow–broad band colour diagram

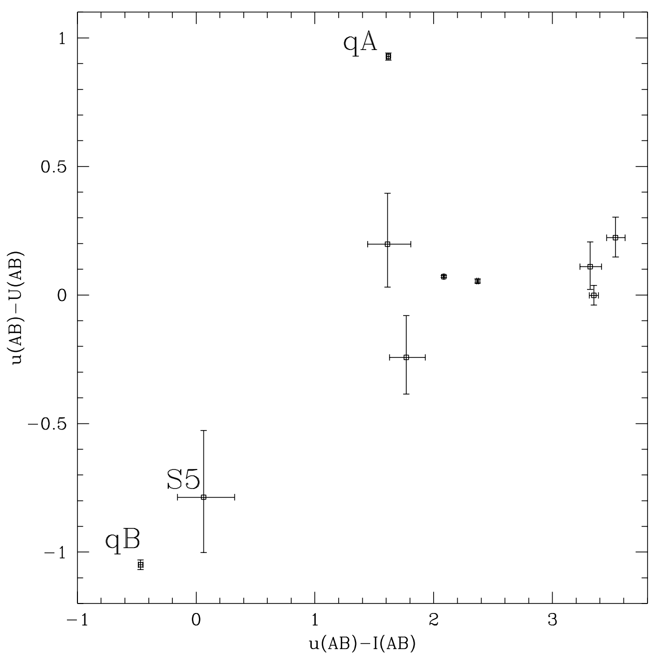

Figure 3.4: $u_{AB} - U_{AB}$ vs. $u_{AB} - I_{AB}$ for 10 objects detected at a signal-to-noise ratio larger than 4. Marked are the two quasars qA and qB and an emission line candidate S5.

The purpose of the broad band imaging of the field is to use the $u_{AB} - U_{AB}$ colour to point out candidate Lyα emitters and secondarily if possible to obtain broad band fluxes and colours of eventual discovered candidates. An object with Lyα emission at z=1.93 will appear bright in u_{AB} compared to U_{AB} and I_{AB}. Thus in a u_{AB}–U_{AB} vs. u_{AB}–I_{AB} colour diagram it will lie in the lower left corner. Conversely an object with absorption in the narrow filter will appear to be faint in u_{AB} compared to U_{AB} and I_{AB}, and in a u_{AB}–U_{AB} vs. u_{AB}–I_{AB} colour diagram it will lie in the upper right corner.

We use the sum of the three combined images I,U and narrow as a detection image for SExtractor. SExtractor then uses the exact same isophotes for all three filters. As a detection filter we approximate the PSF of the summed image with a gaussian, which is optimal for detection of faint sources. We then

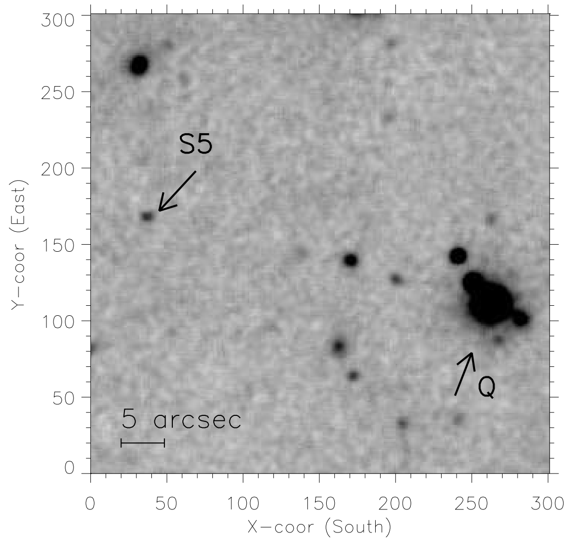

Figure 3.5: The emission line candidate S5 and the two quasars Q.

measure the flux in each of the three individual frames and the corresponding noise from the noise images produced in the combination process for all detected objects (see section 3.2.2).

In Fig. 3.4 we show a narrow–broad band colour diagram for all objects detected at a signal-to-noise ratio large than 4 in the narrow-band frame. Seven objects are found to have u_{AB}–$U_{AB} \approx 0$ corresponding to no special features in the narrow filter compared to U. Due to the damped Lyα absorption line qA lies in the upper part of the diagram with u_{AB}–U_{AB} = 0.93. This is even an underestimate of u_{AB}–U_{AB} since in the narrow band frame the emission from S4 is added to that of qA by SExtractor. Subtracting the narrow-band emission due to S4 leads to u_{AB}–U_{AB} = 1.22 for qA. qB lies in the lower left part of the diagram, thus we conclude that qB is not absorbed by S4 and that it has Lyα in emission. Also, in the lower left part of the diagram is the galaxy marked S5 in Fig. 3.2. S5 is an excellent emission line candidate. It is detected at a signal-to-noise ratio of 4.8 in narrow-band, and 13 and 14 in the I and U frames respectively. The Lyα flux from S5 is 6.5(1.3) x 10^{-17} erg cm^{-2} s^{-1} from the isophotal magnitude. Fig. 3.5 shows 300x300 pixels (53x53 arcsec^2) containing S5 and the two quasars. S5 is marked north east of the QSOs. The projected distance of S5 from qA is 40.9 arcsec, which assuming q_0=0.5, H_0 = 100h km s^{-1} Mpc^{-1} and $\Lambda = 0$ corresponds to 169 h^{-1} kpc.

The u_{AB} magnitude of S4 is 20.49±0.05. Assuming that all the residual emission in the PSF subtracted U frame originates from S4 leads to an upper limit for its u_{AB}–U_{AB} colour of -1.5, thus placing it it in the lower left corner of Fig 3.4.

3.4 Discussion

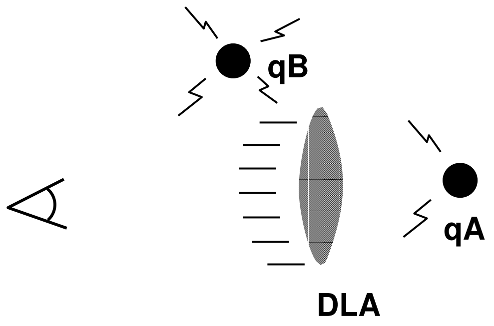

Figure 3.6: The suggested geometry

The extent of the Lyα emitting region is 24x12h^{-2} kpc^2. The line measured flux is 1.88(4)x10^{-15} ergs cm^{-2} s^{-1}, which corresponds to a luminosity of 1.19(3)x10^{43}h^{-2} ergs s^{-1}. Table 3.1 shows the emitted Lyα fluxes and luminosities of the other three DLAs in the literature with detected emission. Table 3.1 shows that the Lyα luminosity of S4 towards qA is an order of magnitude higher than what is found from other DLAs. This suggests that the source of ionization might be different for this DLA. In Fig. 3.6 is shown the suggested geometry of the system. We suggest that qB is ionising the side of S4 facing us. To derive the maximum distance between qB and S4 under this hypothesis we assume that the spectrum of qB can be modelled by a power law $f_\nu \propto \nu^{-\alpha}$ and that case B recombination produces the Lyα photons. This is valid for optically thick clouds [25]. In case B recombination 68% of all photons below the Lyman limit produce a Lyα photon. For the geometry above we assume an angle ϕ between the normal of the plane of S4 and the line from qB to S4, a distance d between the two objects and an area S of S4. We determine the slope α from the I_{AB} and U_{AB} magnitudes to be

$$\alpha = \frac{2}{5}(I_{AB} - U_{AB})log(\frac{360nm}{800nm})^{-1} = 0.8.$$

The expected Lyα luminosity of S4 is then

$$L(Ly\alpha) = 0.68\frac{F_\nu(\frac{3600\mathring{A}}{1+z_{qB}})}{h\alpha}\left(\frac{(1+z_{qB})912}{3600}\right)^\alpha \frac{hc}{1216\mathring{A}}\frac{Scos(\phi)}{4\pi d^2},$$

and the Lyα flux is then given by

$$f(Ly\alpha) = 0.682\frac{f_\nu(3600\mathring{A})}{h\alpha}\left(\frac{(1+z_{qB})912}{3600}\right)^\alpha \frac{hc}{1216\mathring{A}}\frac{Scos(\phi)}{4\pi d^2}.$$

DLA	Reference	z_{DLA}	Measured Flux ergs s^{-1} cm^{-2}	Luminosity ergs s^{-1}
S1	Møller & Warren [12],[13]	2.81	7.4x10^{-17}	1.10h^{-2}x10^{42}
DLA2059–360	Pettini et al. [15]	3.08	7x10^{-17}	1.3h^{-2}x10^{42}
DLA2233+131	Djorgovski et al. [14]	3.15	6.4x10^{-17}	1.23h^{-2}x10^{42}

Table 3.1: Lyα fluxes and luminosities.

Assuming $\cos(\phi)$=0.5 we then find for d

$$d \lesssim 40h^{-1}kpc.$$

For comparison the distances to our 5 nearest neighbours in the local group are between 50 and 85 kpc [26], thus $40h^{-1}$ kpc is a reasonable intergalactic distance.

If this interpretation is correct, what we see is the full outline of the HI-cloud causing the damped absorption line in the spectrum of qA.

3.4.1 Comparison with the Lyman-break Galaxies

The size of the HI cloud is surprisingly large compared to the very compact Lyman–break galaxies which have half-light radii smaller than 2 kpc [30]. However, the Lyman–break galaxies are often embedded in more extended and diffuse halos [30]. It might be that generally the regions of star formation in young galaxies are very compact knots, but that the distribution of the gas is much more extended. This has also been suggested in [34] where from deep HST imaging in the field of PKS0528-250 the authors observe that the Lyα emission contours from S1, S2 and S3 are more extended than in broad band.

It is very interesting to compare the sample of Lyman-break galaxies with the DLAs. The two groups suffer from widely different selection biases. The Lyman-break galaxies are all very luminous with absolute magnitudes M<-21. The space density, as inferred from the Hubble Deep Field (HDF) by Lowenthal et al. [28], of (8.8–13)x10^{-3}h^3 Mpc^{-3} is comparable to that of L>L* galaxies in the local universe. The space density n_{DLA} of DLAs can be inferred from the observed redshift density through the relation (see for example [29])

$$\frac{dN}{dz} = \frac{\pi r_{DLA}^2 c n_{DLA}}{H_0}(1+z)(1+2q_0 z)^{-1/2},$$

where r_{DLA} is the typical radii of DLAs. $\frac{dN}{dz}$ has been measured by several investigators, for example [5] and [7], thus given a cosmological model the product $\pi r_{DLA}^2 n_{DLA}$ can be derived. Knowing r_{DLA} would allow us to derive n_{DLA}. However, we do not know r_{DLA}. *Assuming* that DLAs have typical radii r_{DLA} of 10 kpc and using the measured redshift density of DLAs [5], [7] we find that $n_{DLA} \approx 2\text{x}10^{-1}$ h^3 Mpc^{-3}. This is about 15 times higher than that of Lyman-break galaxies in the HDF, meaning that more than 90% of the DLAs are either not Lyman–break galaxies or have broad band fluxes fainter than the selection limit of $(V_{606}+I_{814})/2$ = 25.5 applied by Lowenthal and collaborators (V_{606} and I_{814} are the HST V and I filters). This space density of DLAs is about 3-4 times larger than the integrated luminosity function of 5.3x10^{-2} h^3 Mpc^{-3} derived from the Las Campanas Redshift Survey [31]. This would mean that a considerable amount of merging has brought us from the objects at high redshift to present day galaxies. However, this discussion is still purely academic, since we do not know as yet the typical sizes of DLAs. More observations are required.

Chapter 4

Outlook

In the following sections I outline the projects I will be working on in part B of my PhD study. Primarily we have applied for observing time with the purpose to detect Lyα from more high column density QALS. Since now three out of four DLAs with detected emission are $z_{abs} \approx z_{ems}$ systems we have chosen to study mainly this special subgroup of the QALS. We also hope to obtain further insight into the nature of $z_{abs} \approx z_{ems}$ absorbers by performing a statistical study of DLAs in the literature.

First I describe the observational projects.

4.1 Further studies of Q0151+048

4.1.1 Deconvolution

As mentioned in chapter 3 there is an open question concerning the significance of the residuals after PSF-subtraction of qA in the U combined frame. To address this question we have contacted a Belgium group, Pierre Magain and collaborators, who have developed a deconvolution code, i.e. a code that improves the resolution of the image by deconvoluting with a well chosen function, see e.g. [40]. We hence gave them our U-band data so that they code run their code on it. Preliminary results are very promising, and Pierre Magain writes : " *We have no reasonable doubts about the reality of the diffuse component superimposed on the brightest image* (qA, my comment).' I hope to visit Pierre Magain at the Institut d'Astrophysique in Liege in February 1998 to complete this analysis.

4.1.2 Follow-up Spectroscopy

In 1996, Palle Møller, Stephen J. Warren and I (PI Fynbo) applied for observing time for follow-up spectroscopy of S4 at NOT. We were granted three nights in September 1997. We had three nights of data, unfortunately, with rather poor seeing around 1.5-2 arcsec FWHM. However, this data will provide us with very important information about the nature of S4, in particular concerning the kinematics of the gas. We intended to look for the rotation curve of the galaxy, which if successful would be the first rotation curve to be seen at z>1. We hence aligned a slit with the major axis of the galaxy. A preliminary reduction of the data confirms the extended emission seen in the narrow band data, and it also shows signs of velocity fields, however, *not* compatible with simple rotation of a disc. We need more and better data to fully understand this system. Hence, we will apply for observing time for further spectroscopy in October 1998 on NOT and/or the Very Large Telescope (VLT).

4.2 PKS1157+014, NOT, March 98

For 1998 we have obtained observing time for two projects. The first of these projects concerns the $z_{abs} = 1.9436$ DLA towards the $z_{ems} = 1.978$ quasar PKS1157+014, that is ideally suited for our study of $z_{abs} \approx z_{ems}$ DLAs. Palle Møller, Bjarne Thomsen and I (PI Fynbo) then applied for and were granted 4 nights of observing time on the NOT for a narrow/broad study of this system.

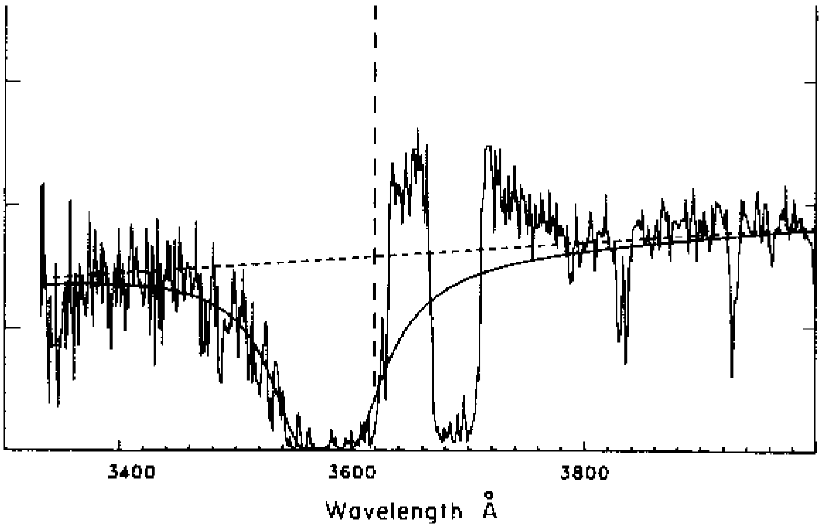

Figure 4.1: The Lyα region in the spectrum of PKS1157+014. The units on the y-axis are arbitrary flux units.

As in the case of PKS0528–250 the Lyα emission line from the quasar is absorbed by a DLA with a redshift close to the emission redshift of the quasar. The column density of the DLA is 21.8 which is extremely high. We have not found any DLA with higher column density in the literature. Fig 4.1 shows the Lyα region in the spectrum of PKS1157+014 from [43]. Shown is the flux from the quasar in arbitrary units as a function of wavelength. The full drawn line shows a fit to the strong damped profile with a column density N(HI) = 6.1×10^{21} cm^{-2} at a redshift z = 1.94362. The short dashed curve shows a fit to the continuum, and the vertical long dashed line indicates the redshift z = 1.978(8) of the quasar. The strong absorption trough redwards of the damped Lyα line is due to NV in a highly ionized intrinsic absorber, i.e. an absorber that is related to the QSO itself. The system giving rise to the damped Lyα absorption line is also detected in redshifted 21 cm absorption, which is possible since PKS1157+014 is a strong radio emitter.

We have designed and ordered a 25Å narrow filter for a narrow/broad band study of this DLA.

4.3 Q1205–30, NTT, March 98

The second project for which we have been granted observing time in 1998 is concerned with a $z_{abs} \approx z_{ems}$ Lyman limit system towards the $z_{ems} = 3.036$ QSO Q1205–30. Lyman limit absorbers are objects with HI column density high enough that the optical depth for Lyman limit absorption is of order unity or higher. This corresponds to $N_{HI} \gtrsim 10^{17}$ cm^{-2}. This object was chosen by Palle Møller based on the published spectrum in [41]. Based on the Lyα absorption line the column density of this absorber can be estimated to be $\approx 10^{19}$ cm^{-2}.

Palle Møller, Bjarne Thomsen and I (PI Fynbo) then applied for observing time on the ESO 3.5m NTT telescope. We were granted 20 hours category B service observing time.

4.3.1 Obtaining the coordinates of Q1205–30

We soon realized that the coordinates of Q1205–30 have never been published. In [41] the reference is 'McMahon and Hazard, unpublished'. I searched the literature for all references to this QSO finding no coordinates. I then contacted Dr. Richard G. McMahon at the Institute of Astronomy in Cambridge and asked very politely whether the coordinates of Q1205–30 had been published or could be made available. He, however, never replied. We consequently had to 'rediscover' Q1205–30 somehow. It turned out that the Royal Observatory in Edinburgh has a prism plate survey covering the relevant area of the southern

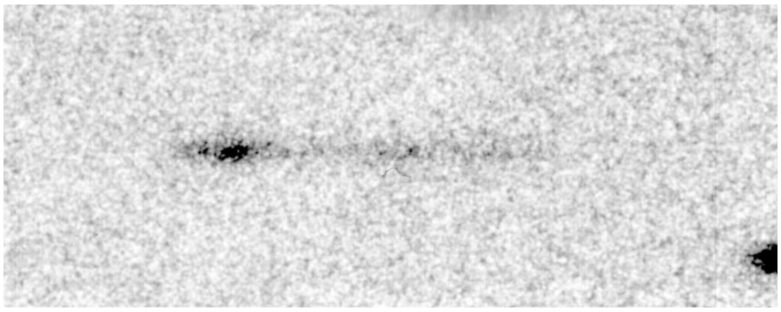

Figure 4.2: The prism-plate spectrum of the object we believe is Q1205–30.

sky. It was possible to get a copy of a given plate, and with splendid help from the staff at the Royal Observatory we succeeded in finding the QSO, or at least a very good candidate for it. Fig. 4.2 shows the prism-plate spectrum of the object we believe is Q1205–30. The emission line in the left side of the spectrum would be at the correct redshift of redshifted Lyα. Through the digital sky survey [42] we then identified the object and measured the coordinates to be : 12 05 35.722, -30 14 25.8 (1950).

4.4 Q0027+0103, NOT, September 98?

Are $z_{abs} \approx z_{ems}$ DLAs really more likely to be Lyα emitters or is the fact that three out of four DLAs with detected Lyα emission are $z_{abs} \approx z_{ems}$ systems only coincidental? Our success in detecting Lyα emission from $z_{abs} \approx z_{ems}$ DLAs could just be due to superior data compared to that of unsuccessful groups. As an example, the many null detections in a paper by Lowenthal et al., [11], were all obtained in rather poor seeing conditions compared to the NOT standard, with a median seeing of 2.5 arcsec. The only $z_{abs} << z_{ems}$ DLA in the literature with Lyα emission, DLA2233+131, was detected using the 10m Keck telescope in good seeing. Using NOT with 1 arcsec seeing in 4 nights we would also be able to detect this DLA.

In order to test whether $z_{abs} \approx z_{ems}$ DLAs are more likely Lyα emitters we have applied for observing time for a narrow/broad band study of a $z_{abs} << z_{ems}$ DLA under exactly the same conditions as for the case of the study of the $z_{abs} \approx z_{ems}$ DLA S4. In order to do this experiment we searched the literature for DLAs at redshifts very close to that of S4, z = 1.9342, so that we could use the same narrow-band filter.

By far the best candidate found is the DLA towards Q0027+0103 [5]. The redshift of this DLA is z = 1.9375, hence, eventual Lyα emission at λ = 3571 Å from this DLA will sit perfectly near the centre of the 20Å narrow-band filter designed for S4 (see Fig. 3.1). The HI column density of the DLA is log(HI) = 20.6, which is very similar to that of S4, log(HI) = 20.4.

Palle Møller, Bjarne Thomsen and I (PI Fynbo) have applied for 4 nights for this project. If we are granted the time we will observe this system in September 1998.

4.5 HST-STIS and NICMOS surveys for emission from DLAs

Palle Møller and Collaborators have obtained observing time for a survey aimed at obtaining emission from a large, unbiased sample of DLAs with both STIS (Space Telescope Imaging Spectrograph) and NICMOS (Near Infrared Camera and Multi Object Spectrometer) on HST. Q0151+048 will be among the DLAs in this sample, and I will in particular be working with the HST-data for this object.

4.6 Anti-correlation between column density and impact parameter

If we succeed in detecting emission from PKS1157+014 and Q1205–30 we will have in our sample of DLAs emission objects with HI column density ranging from 10^{19} cm^{-2} to 6x10^{21} cm^{-2}. When furthermore all the data from the HST-survey become available we will have a large sample of DLAs with detected emission. We then expect to see an anti-correlation between the impact parameter of the emission region and the column density of the absorber. The precise manner in which the DLAs distribute themselves in a plot of impact parameter versus column density will give us detailed information about the sizes of DLAs, see [34]. This can be understood in the following way. Assume that all DLAs are identical rotationally symmetric discs with a characteristic decline of HI density as a function of distance from the disc centre. The different HI-column densities observed in the QSO spectra would then result from the different ways the line of sight passes through the disc. More specifically DLAs with a small impact parameter to the QSO would produce a stronger absorption than a DLA with a large impact parameter. From the column density vs. impact parameter diagram one would be able to determine the characteristic shape of the DLAs. Real DLAs of course display a range of shapes and sizes, but still from the column density vs. impact parameter diagram we can determine the average.

4.7 Are $z_{abs} \approx z_{ems}$ Absorbers Overabundant?

Let me now turn to the literature study we plan to do. Weymann and collaborators in 1979 performed a study of the statistics of the incidence of QALS giving rise to CIV and MgII absorption as a function of $z_{ems}- z_{abs}$ [44]. They found that these QALS could be divided into three subgroups : 1) intervening absorbers, 2) absorbers due to gas ejected from the QSO, and 3) a cluster component which is somehow related to the cluster in which the galaxy hosting the QSO is assumed to be a member. The third group shows a velocity dispersion around z_{ems} which is comparable to that of galaxies in clusters. This study is based on a survey of small and intermediate redshift QSOs ($0.40 < z_{ems} < 1.95$).

The question is now whether DLAs also show an overabundance near z_{ems}, i.e. if we can find a sign of clusters in the DLA statistics. To try to answer this question we will, based on the published catalogs of DLAs, form a large sample for a statistical analysis. It is not yet obvious whether this study is possible since it may be very difficult to compensate for selection effects. As an example of a such selection effect many QSOs are found using low dispersion spectroscopy. QSOs with $z_{abs} \approx z_{ems}$ completely lack the Lyα emission line which normally is the characteristic feature of high-z QSO spectra, see e.g. Fig 4.2. Thus there might be a bias against finding such QSOs. QSO catalogs based on radio-emission or broad band colours on the other hand are not influenced by this bias.

4.8 Projects for the VLT

In 1998 the first of the four 8m telescopes of the VLT will be made available. It is obvious that we will benefit from this. The first instruments that become available in 1998 are FORS (FOcal Reducer/low dispersion Spectrograph) and ISAAC (Infrared Spectrometer And Array Camera). With FORS we will be able to perform both spectroscopy and imaging in the near UV. Hence this instrument will be perfectly suited for further studies of the z $\approx$ 1.9 objects in the fields of Q0151+048, PKS1157+014 and Q0027+0103, all of which can be reached with VLT at Paranal. The infrared instrument ISAAC will be interesting for spectroscopic purposes. For high redshift objects the prominent Balmer lines and strong oxygen lines are found in the infrared, hence ISAAC will be of interest for studies of the physical conditions in the gas inside DLAs.

4.9 Summary

Understanding the nature of Damped Lyα Absorbers (DLAs) is of large importance in the understanding of how present day galaxies were formed. Being candidate (proto-)galaxies at high redshifts, the determination of size, morphology, and state of star formation of this class of objects is one of the crucial missing pieces in our understanding of the evolution from primordial fluctuations to present day spiral and elliptical galaxies. The main goal of this PhD study has been and will be to collect observations that will help this missing piece to find is proper place in the puzzle of galaxy formation.

Bibliography

[1] D.J. Fixen, E.S. Cheng, J.C. Mather, R.A. Shafer, and E.L. Wright, ApJ, 1996, 473, 576

[2] T. Kim, E.M. Hu, L.L Cowie, A. Songaila, 1997, AJ, 114, 1

[3] E.M. Hu, T. Kim, L.L. Cowie, A. Songaila, and M. Rauch, 1995, AJ, 110, 1526

[4] Gardner J.G., Katz N., Weinberg D.H., Hernquist L., 1997, preprint (Astro-ph/9705118)

[5] Wolfe A.M., Lanzetta K.M., Foltz C.B., and Chafee C.H., 1995, ApJ, 454, 698

[6] K.M. Lanzetta, A.M. Wolfe,D.A. Turnshek, 1995, ApJ, 440, 435

[7] Storrie-Lombardi L.J., Irwin M.J., and McMahon R.G., 1997, MNRAS, 283, L79

[8] A. Songaila and L.L. Cowie, 1996, AJ, 112, 335

[9] Lu L., Sargent W.L.W., Barlow T.A., Churchill C.W., and Vogt S.S., 1996, ApJS, 107, 475

[10] Haehnelt M.G., Steinmetz M., and Rauch M., 1997, preprint (http://xxx.sissa.it/abs/astro-ph/9706201)

[11] Lowenthal J.L., Hogan G.J., Green R.F., Woodgate B., Caulet A., Brown L., and Bechthold J., 1995, ApJ, 451, 484

[12] Møller P., Warren S.J., 1993, A&A, 270, 43

[13] Warren S.J., Møller P., 1996, A&A, 311, 25

[14] Djorgovski S.G., Pahre M.A., Bechtold J., and Elston R., 1996, Nature, 382, 234

[15] Pettini M., Hunstead R.W., King D.L., and Smith L.J., 1995, In: Meylan G. (ed.) QSO Absorption Lines, Springer-Verlag, Berlin, p.55.

[16] Steidel C.C., Pettini M., Dickinson M, and Persson S.E., 1994, AJ, 108, 2046

[17] Aragón-Salamanca A., Ellis R.S., and O'Brien K., 1996, MNRAS, 281, 945

[18] Le Brun V., Bergeron J., Boissé P., and Deharveng, 1997, A&A, 321, 733

[19] Møller P., Warren S.J., and Fynbo J.U., 1997, A&A, accepted

[20] Williams R.E., and Weyman R.J., 1976, ApJ, 207, L143

[21] Landolt A.U., 1992, AJ, 104, 340

[22] Oke J.B., 1990, AJ, 99, 1621

[23] Colina L., Bohlin R.C., 1994, AJ, 108, 1931

[24] Fukugita M., Shimasaku K., and Ichikawa T., 1995, PASP, 107, 945

[25] See e.g. Osterbrock D.E., 1989, In "Astrophysics of Gaseous Nebulae and Active Galactic Nuclei", (University Science Books), p. 77.

[26] Allen C.W., 1973, 'Atrophysical Quantities', (The Athlone Press), p.287.

[27] Pettini M, Steidel C.C., Adelberger K.L., Kellogg M., Dickinson M., and Giavalisco M., 1997, preprint (astro-ph/9708117)

[28] Lowenthal J.D., Koo D.C., Guzman R., Gallego J., Phillips A.C., Faber S.M., Vogt N.P., Illingworth G.D., and Gronwall C., 1997, ApJL, 481, 673

[29] Peterson, B.M., 1997, 'Active Galactic Nuclei', (Cambridge University Press), p. 206

[30] Giavalisco M., Steidel C.C., Macchetto F.D., 1996, ApJ, 470, 189

[31] Lin H., Kirshner R.P., Shectman S.A., Landy S.D., Oemler A., Tucker D.L., Schechter P.L., 1996, ApJ, 464, 60

[32] Morton D.C., Jian-sheng C., Wright A.E., Peterson B.A, and Jauncey D.L., 1980, MNRAS, 193, 399

[33] York D.G., Yanny B., Crotts A., Carilli C., Garrison E., and Matheson L., 1991, MNRAS, 250, 24

[34] Møller P. and Warren S.J., 1997, MNRAS, submitted

[35] Holztman J.A., Burrows C.J., Casertano S., Hester J.J., Trauger J.T., Watson A.M., and Worthey G., 1995, PASP, 107, 1065

[36] Bertin E. and Arnouts S., 1996, A& AS, 117, 393B

[37] Bruzual A.G. and Charlot S., 1993, ApJ, 405, 538

[38] Møller P. and Jakobsen P., 1990, A&A, 228, 299

[39] Madau P., 1995, ApJ, 441, 18

[40] Magain P., Courbin F., and Sohy S., 1997, *The Messenger*, 88, 28

[41] Lanzetta K.M., Wolfe A.M., Turnshek D.A., Lu L.,McMahon R.G., Hazard C., 1991, ApJS, 77, 1

[42] http://arch-http.hq.eso.org/cgi-bin/dss

[43] Briggs F.H., Turnshek D.A., and Wolfe A.M., 1984, ApJ, 287, 549

[44] Weymann R.J., Williams R.E., Peterson B.M., and Turnshek D.A., 1979, ApJ, 234, 33